

1  
2  
3  
4  
5  
6  
7  
8  
9  
10  
11  
12  
13  
14  
15  
16  
17  
18  
19  
20  
21  
22  
23  
24  
25

# **Noise in the Cretaceous Quiet Zone uncovers plate tectonic chain reaction**

**Authors:** Derya Güler<sup>1,2</sup>, Roi Granot<sup>3</sup>, Douwe J J van Hinsbergen<sup>1</sup>

<sup>1</sup> Department of Earth Sciences, Utrecht University, 3584 CD Utrecht, The Netherlands

<sup>2</sup> School of Earth and Environmental Sciences, University of Queensland, St. Lucia, QLD 4072, Australia

<sup>3</sup> Department of Earth and Environmental Sciences, Ben-Gurion University of the Negev, Beer-Sheva 84105, Israel

e-mails: [derya.guerer@uq.edu.au](mailto:derya.guerer@uq.edu.au), [rgranot@bgu.ac.il](mailto:rgranot@bgu.ac.il), [d.j.j.vanhinsbergen@uu.nl](mailto:d.j.j.vanhinsbergen@uu.nl)

Twitter: @geoceanic (Derya Güler), @vanHinsbergen (Douwe van Hinsbergen)

*This manuscript is a non-peer reviewed preprint submitted to EarthArXiv.*

***Manuscript under consideration at Nature Geoscience***

*Original submission date: 13th May 20*

Correspondence and requests for materials should be addressed to DG, [derya.guerer@uq.edu.au](mailto:derya.guerer@uq.edu.au)

26 **Noise in the Cretaceous Quiet Zone uncovers plate tectonic chain**  
27 **reaction**

28

29 Derya Gürer<sup>1,2\*</sup>, Roi Granot<sup>3</sup>, Douwe J J van Hinsbergen<sup>1</sup>

30

31 **Global plate reorganizations, intriguing but loosely defined periods of profoundly changing plate**  
32 **motions, may be caused by a single trigger such as a continental collision or a rising mantle plume.**  
33 **But whether and how such triggers propagate throughout a plate circuit remains unknown. Here,**  
34 **we show how a rising mantle plume set off a ‘plate tectonic chain reaction’. Plume rise has been**  
35 **shown to trigger formation of a subduction zone within the Neotethys Ocean between Africa and**  
36 **Eurasia at ~105 Ma. We provide new constraints on Africa-Eurasia convergence rates using**  
37 **variations in geomagnetic ‘noise’ within the Cretaceous Normal Superchron (the 126-83 Ma period**  
38 **without magnetic reversals) recorded in the Atlantic Quiet Zones crust. These new constraints are**  
39 **consistent with the timing of numerically predicted African Plate acceleration and deceleration**  
40 **associated with onset and arrest of the intra-Neotethyan subduction zone. The acceleration was**  
41 **associated with a change in Africa-Eurasia convergence direction, which in turn was**  
42 **accommodated by a next subduction initiation at ~85 Ma in the Alpine region that cascaded into**  
43 **regional tectonic events. Our concept of plate tectonic chain reactions shows how changes in plate**  
44 **motion, underpinned by mantle dynamics, may self-perpetuate through a plate circuit, making**  
45 **global plate reorganizations a key to unlock the driving mechanisms behind plate tectonics.**

46

47 Pronounced changes in the velocity and/or direction of tectonic plate motions are short-lived events  
48 punctuating long periods of gradually evolving motion<sup>1-3</sup>. Inspection of global plate kinematic models  
49 and of geological records at plate boundaries have led to the hypothesis that plate motion changes are at  
50 times concentrated in ‘global plate reorganizations’: short-lived but ill-defined periods of ~10 Ma in

51 which plate motions change across the globe. Such reorganizations, for instance in the mid-Cretaceous  
52 around 105 Ma<sup>2-4</sup> or in the Eocene, around 50 Ma<sup>5-8</sup>, are suspected to be triggered by geodynamic  
53 coincidences such as rising mantle plumes<sup>2</sup>, collisions<sup>2-5</sup>, or ridge subduction<sup>6-8</sup>. But to set off a global  
54 plate reorganization, plate motion changes induced by such isolated dynamic triggers must be able to  
55 cascade to neighbouring plates, for which a mechanism has so far not been identified.

56 We hypothesize that when a trigger causes a plate motion change, this change may in turn trigger  
57 subsequent plate motion changes, in what we conceptualize as a ‘plate tectonic chain reaction’.

58 Geodynamic analysis has long identified that the main drivers of plate motion are the negative buoyancy  
59 of subducted lithosphere (slab pull), and occasional short-lived and subtle effects of spreading mantle  
60 plume heads below the lithosphere (plume push<sup>9-11</sup>). Formation of new, or the abandonment of pre-  
61 existing plate boundaries (mid-oceanic ridges or subduction zones), at times combined with the arrival of  
62 mantle plumes, are thus widely regarded to form the dynamic underpinning of observed plate motion  
63 changes<sup>7,9-15</sup>. Initiation of subduction of a plate, either spontaneously<sup>16</sup> or forced (for instance by ridge  
64 subduction<sup>7,17</sup>, or by arrest, relocation, or reversal of subduction) will change where and on which plates  
65 slab pull is exerted<sup>14</sup>. The onset or cessation of a slab pull force after initiation or arrest of subduction is,  
66 in turn, a logical driver of plate acceleration or deceleration, respectively<sup>7,13,14,17</sup>. Hence, while initiation  
67 of a new subduction zone may respond to an initial trigger, for instance plume push<sup>18,19</sup>, such initiations  
68 may also be forced by (the dynamic processes underlying) cascading plate motion changes. Subduction  
69 initiation events may thus form the links making plate tectonic chain reactions possible.

70 Recently, the study of ophiolites in Oman and Anatolia revealed that the formation of an intra-oceanic  
71 subduction zone around 105 Ma was forced by far-field stress changes<sup>18</sup>. This subduction zone formed in  
72 the Neotethys Ocean in the modern eastern Mediterranean region and continued to the western Indian  
73 Ocean, where it transitioned into a spreading ridge between India and Madagascar<sup>11</sup>. Its formation is  
74 proposed to result from the push of the Morondava plume head (Fig. 1b) causing a India-Africa plate  
75 motion change at ~105 Ma<sup>11</sup>. By 96-92 Ma, this subduction zone developed sufficient slab pull to drive  
76 upper plate extension widely recorded in the age of the crust of supra-subduction zone ophiolites from the

77 Mediterranean region to Oman and Pakistan<sup>18</sup>. Because forced initiation and development of significant  
78 slab pull are separated by ~10 Ma, this provides the opportunity to separate the dynamic causes from the  
79 consequences of this subduction zone, making this the ideal test case to evaluate the plausibility of plate  
80 tectonic chain reactions. To identify potential causes of subduction initiation, we explore kinematic  
81 predictions of generic numerical models to evaluate whether this onset of slab pull may in turn have been  
82 a trigger of a subsequent plate motion change, and whether this change caused another plate boundary  
83 reorganization, thus defining a chain reaction. But to do this, required overcoming a notorious problem:  
84 the absence of plate kinematic constraints during the Cretaceous Normal Superchron (CNS), the 126-83  
85 Ma<sup>20</sup> period without magnetic polarity reversals expressed in the oceanic Cretaceous Quiet Zone (CQZ)  
86 crust. Therefore, we calculated the first Africa-Eurasia kinematic plate model for the CNS using recently  
87 identified magnetic intensity variations on the Atlantic CQZs<sup>21</sup>. This paved the path to analyze the  
88 dynamic propagation of plate tectonic chain reaction, that may be part of the enigmatic Cretaceous plate  
89 reorganization.

90

### 91 **Global plate reorganizations and proposed triggers**

92 The two most widely discussed global plate reorganizations are the Cretaceous (~105-100 Ma)<sup>2</sup> and  
93 Eocene (~55-45 Ma)<sup>5</sup> plate reorganizations. The Cretaceous reorganization, during the CNS, was inferred  
94 based on changes in the Atlantic, Indian, and northern Pacific fracture zone orientations<sup>2</sup>. The age was  
95 loosely estimated based on interpolation of seafloor spreading rates, and further defined by inspection of  
96 tectonic events recorded in continental geological records across the globe in the 110-90 Ma time period<sup>2</sup>.  
97 Tectonic shortening in western North America and East Asia, subduction along western South America,  
98 extension in Antarctica and Australia, and basin instability in Africa and Europe were all used to identify  
99 this reorganization<sup>2</sup>. Proposed triggers include cessation of subduction along the east Australian-New  
100 Zealand margin due to collision of the Hikurangi oceanic plateau<sup>2</sup>, the rise of the Bouvet mantle plume in  
101 the South Atlantic Ocean<sup>2</sup>, collision between microcontinents in Tibet<sup>4</sup>, and the formation of an Andean-

102 style subduction zone along continental Eurasia<sup>3</sup>. But how these triggers would have propagated to cause  
103 changes ascribed to the reorganization remains undefined.

104 Similar to the Cretaceous reorganization, the Eocene plate reorganization is hypothesized based on a  
105 series of plate kinematic changes across the globe including the Pacific plate motion change reflected by  
106 the prominent change in the Hawaii-Emperor seamount chain, the formation of subduction zones, mid-  
107 ocean ridges, back-arc basins, and orogens<sup>5,8,22-26</sup>, yet it remains unclear whether this was the response to  
108 one single or multiple unrelated triggers, or how these kinematic changes dynamically propagated in  
109 space and time. Proposed drivers for all or part of the reorganization include initiation of Pacific Plate  
110 subduction, either spontaneously<sup>16</sup>, by ridge subduction<sup>7,8,17</sup> or subduction polarity reversal<sup>14</sup>, collision of  
111 India and Asia<sup>5</sup>, collisions and subduction relocation in western North America<sup>27</sup>, and lower mantle  
112 subduction of slabs below South America<sup>28</sup>.

113

#### 114 **Intra-Neotethyan subduction initiation: start of a tectonic chain reaction?**

115 We test our concept of a plate tectonic chain reaction through a case study of the initiation of a major  
116 intra-oceanic subduction zone in the Neotethys Ocean. During the mid-Cretaceous, an intra-oceanic  
117 subduction zone formed from a trench-trench-trench triple junction with a subduction zone that had  
118 already existed since Jurassic time along the southern Eurasian margin<sup>19,22</sup> to the west Indian Ocean,  
119 where the plate boundary transitioned into a rift (and later ridge) that ended in a ridge-ridge-ridge triple  
120 junction in the Southern Ocean<sup>11</sup>. This initiation of the intra-Neotethyan subduction zone generated a so-  
121 called double, in-line subduction zone configuration between Africa and Eurasia and formed a new plate  
122 consisting predominantly of Neotethyan oceanic lithosphere<sup>23</sup> (Fig. 1b). In the latest Cretaceous, the  
123 southern rim of this plate was emplaced onto continental crust of Greater Adria, Africa, and Arabia along  
124 the southern Neotethyan margin (black hatched area in Fig. 1c) and relics are today preserved as forearc  
125 supra-subduction zone ophiolites in the eastern Mediterranean region and along northeastern Arabia, and  
126 in melanges in suture zones<sup>22,24,25</sup> (Fig. 1d). Geochemical and geochronological data show that the  
127 formation of oceanic crust of these ophiolites, due to upper plate extension and seafloor spreading above a

128 nascent subduction zone (so-called ‘supra-subduction zone ophiolites’), began by ~96-95 Ma in Oman<sup>24</sup>  
129 and ~92 Ma in the eastern Mediterranean region<sup>25</sup>. These observations demonstrate that by this time, slab  
130 pull in the new subduction zone was sufficient to rupture the upper plate, and must have exerted slab pull  
131 on the trailing African-Arabian Plate<sup>26,29</sup>. The initiation of the subduction zone itself predated upper plate  
132 extension, and was already underway by 104 Ma as constrained by garnet Lu/Hf geochronology of  
133 metamorphic soles below the Neotethyan ophiolites<sup>18,30</sup>. This demonstrates that convergence initiating  
134 subduction predated upper plate extension, and must have been induced by a change in plate motion  
135 driven by far-field forcing<sup>18</sup>. Structural geological and paleomagnetic observations of metamorphic soles  
136 and supra-subduction ophiolitic crust suggested that incipient convergence was ~E-W directed, highly  
137 oblique to the southern Neotethyan passive margin<sup>26,31</sup> (Fig. 1b). The rise of the Morondava mantle plume  
138 below the southwest Indian Ocean was identified as the likely trigger: plume rise induced radial plume  
139 head spreading that triggered separation of India and Madagascar, whereby the cratonic keels of India and  
140 Africa acted as pivots around which the two plates underwent an opposite rotation causing E-W  
141 convergence in the Neotethys<sup>11</sup>. This convergence triggered subduction initiation parallel to the stepped  
142 continental margin of west India, Arabia, and Greater Adria<sup>11,22,26,31</sup>. Seismic tomographic images show  
143 that even though the convergence driving subduction initiation was highly oblique to the Arabian-Greater  
144 Adriatic margin, it led to a slab, now located in the mid-mantle below Arabia and the eastern  
145 Mediterranean region, that is broadly parallel to the Cretaceous south Neotethyan margin<sup>32</sup>. Along the  
146 African-Arabian margin, the intra-oceanic subduction zone – and hence the associated slab pull – ceased  
147 between the ~85 Ma first arrival of African/Arabian continental crust in the trench and cessation of  
148 ophiolite obduction by ~70 Ma<sup>22,33</sup> (Fig. 1c).

149 To evaluate whether the inception of slab pull in the new subduction zone may have been a trigger for a  
150 subsequent plate motion change, we explore numerical models of subduction dynamics. The geometry of  
151 the double, in-line subduction zone configuration between Africa and Eurasia (Fig. 1b), which bears  
152 similarities to the Philippine Sea Plate today, has recently received considerable attention in the numerical  
153 modelling community, who predicted that the onset and arrest of double slab pull will generate

154 pronounced plate accelerations and decelerations, respectively<sup>12,34–37</sup>. Convergence rates across coupled  
155 double subduction systems are predicted to be significantly faster than across a single subduction  
156 zone because of the significant slab pull exerted by two slabs working in tandem. Numerical models  
157 suggest that this stronger pull occurs because plates are not decoupled, but appear to “communicate”  
158 through the dynamic pressure build-up in the mantle between them<sup>34</sup>. Numerical models of double, in-  
159 line subduction<sup>12,34–37</sup> thus predict acceleration of Africa-Eurasia convergence rates around ~96-92 Ma  
160 due to onset of double-slab pull, and a deceleration sometime between ~85 and 70 Ma due to subduction  
161 arrest along the Arabian margin. To test that prediction, however, we first need to overcome the crude  
162 temporal resolution of the existing Africa-Eurasia plate kinematic models that stems from the lack of  
163 geomagnetic field reversals during the CNS.

164

#### 165 **Revised Africa-Eurasia plate kinematic model**

166 Past Africa-Eurasia relative plate motions are calculated from restoring the opening of the Central  
167 and North Atlantic Oceans through the Africa-North America-Eurasia plate circuit (Figs. 1 and 2).  
168 Previous reconstructions<sup>38,39</sup>, without any kinematic constraints within the CQZ and without quantified  
169 uncertainties, proposed that Africa moved eastward with respect to Eurasia during the Early Cretaceous  
170 and later rotated northward, sometime during the Cretaceous. These studies also suggested that Africa-  
171 Eurasia convergence rates since the Mesozoic have mostly been stable and small (<20 mm yr<sup>-1</sup>).  
172 Importantly, the lack of geomagnetic polarity reversals between ~126 and 83.6 Ma<sup>20</sup> (i.e., CNS, see  
173 Methods for discussion of the time scale), provides a major challenge for identifying the timing of the  
174 major counter clockwise rotation of Africa relative to Eurasia, and its consequences on the evolution of  
175 convergence rates.

176 We present a revised Africa-Eurasia plate kinematic model that consists of rotation parameters (i.e.,  
177 pole locations, angle of rotations and their uncertainties) for 15 time steps (i.e., magnetic anomalies)  
178 between 156 and 10 Ma, all of which are based on restoring conjugate sets of marine magnetic anomalies  
179 and fracture zone crossings. We compute Africa-Eurasia motion by summing the rotation parameters of

180 Africa-North America and North America-Eurasia (see Methods, Fig. 3, and Extended Data Tables 1 and  
181 2). Next, we overcome the challenge of the lack of polarity reversals during the CNS by tracing two  
182 magnetic anomaly features (Q1 and Q2<sup>21</sup>) that result from prominent changes in the behaviour of the  
183 geomagnetic field (Fig. 2 and Extended Data Fig. 1). Their ages were inferred in the Central Atlantic  
184 CQZs by drill hole data and tectonic constraints at ~92 (Q1) and ~108 (Q2) Ma<sup>21</sup>. Together with  
185 independent seafloor fabric constraints as well as fracture zone crossings, we computed new intra-CNS  
186 finite rotation parameters for Africa-North America motion for Q1 and Q2 and combined them with the  
187 North America-Eurasia rotations. The transition from continental rifting to seafloor spreading between  
188 North America and Eurasia occurred during the CNS<sup>40</sup>, and we cannot confidently identify Q1 or Q2  
189 there. Our analysis assumes that during the CNS the North America-Eurasia motion as indicated by drill  
190 hole data and the relatively simple North Atlantic fracture zone orientations, was ultra-slow and stable  
191 compared to the motion of Africa relative to North America<sup>41</sup>, and combines the Africa-North America  
192 motion with the North America-Eurasia-interpolated rotation parameters for this time period (see  
193 Methods). We note that due to the ultra-slow North America-Eurasia spreading rates this assumption has  
194 minor effects on the resultant Africa-Eurasia motions and associated uncertainties.

195 The new kinematic model (Fig. 3) implies that Africa convergence rates at the easternmost side of the  
196 plate boundary accelerated from low rates of ~20-30 mm yr<sup>-1</sup> prior to the CNS and until Q2, to ~45 mm  
197 yr<sup>-1</sup> averaged over the Q2-Q1 interval (108-92 Ma), followed by a spike at ~70-80 mm yr<sup>-1</sup> between the  
198 Q1 and C33o (92-79.9 Ma) interval. The magnitude of plate acceleration decreases westwards illustrating  
199 that the acceleration coincided with the counter-clockwise rotation of Africa versus Eurasia (Fig. 3b-c).  
200 We note that the spike in convergence rate continued for a brief interval after the CNS (Anomalies C34-  
201 C33o; 83.6-79.9 Ma), independently supporting the intra-CNS results. The spike was followed by a sharp  
202 deceleration at ~80 Ma, after which the convergence rates (Fig. 3c) and the relative plate directions (Fig.  
203 3b) remained relatively stable.

204

205 **Cretaceous plate tectonic chain reaction**

206 The new plate kinematic constraints are consistent with numerical model predictions for plate  
207 kinematic response to double subduction zone inception and arrest<sup>12,34–37</sup>. It is thus feasible that the  
208 acceleration of Africa-Eurasia convergence, and the associated and synchronous counter-clockwise  
209 rotation of Africa, is the dynamic response to the ~96-92 Ma onset of double slab pull. The double slab  
210 pull only affected the eastern half of the African plate and the counter-clockwise rotation of Africa is thus  
211 a logical response. The interpretation that plate motion change is the result of double slab pull is further  
212 supported by the coincidence of arrest of the intra-Neotethyan subduction zone between 85 and 70 Ma<sup>22,33</sup>  
213 (Fig. 1c) and the sharp decrease in convergence rates that we observe (Fig. 3c). This shows that the intra-  
214 Neotethyan subduction zone that was induced from 104 Ma onward by a plume-induced clockwise  
215 rotation of Africa versus India<sup>11</sup>, became itself the driver of the next plate motion change upon inception  
216 of slab pull.

217 Interestingly, the CNS counter-clockwise rotation of Africa relative to Eurasia that we interpret as  
218 driven by the inception of slab pull (Fig. 3), induced convergence on a former transform fault in the  
219 western Mediterranean region. Prior to the rotation, Africa-Iberia and Africa-southern Europe motion was  
220 primarily accommodated along transform faults, but Africa-Eurasia counter-clockwise change in rotation  
221 induced slow convergence that sparked two subduction zones with opposite polarities, straddling from  
222 Iberia to the western Alps<sup>22</sup> (Fig. 1). The oldest high-pressure metamorphic rocks associated with these  
223 new subduction zones, on Corsica<sup>42</sup> and in the western Alps<sup>43</sup>, confirm that subduction was underway by  
224 ~85 Ma. Because convergence rates associated with this subduction were slow (<10 mm yr<sup>-1</sup>, Fig. 3) and  
225 much of the subducting lithosphere in the Alps was continental<sup>22</sup>, the inception of significant slab pull  
226 was long-delayed. For the northwest-dipping slab below Iberia (Fig. 4), roll-back finally led to the  
227 opening of a back-arc basin across the western Mediterranean region from ~30 Ma onward<sup>44</sup>. Roll-back  
228 rates of the south-dipping slab in the western Alps never exceeded African plate advance, and both slabs  
229 were very narrow compared to the plates they were attached to. Thus, the dynamic changes they induced  
230 likely did not cause significant changes in Africa-Eurasia convergence, but were restricted to western  
231 Mediterranean back-arc basin opening<sup>44</sup>. Nonetheless, the chain reaction will likely continue: arrival of

232 the North African lithosphere in the western Mediterranean trench led to subduction arrest some 15 Ma  
233 ago<sup>22</sup>, and ongoing Africa-Europe convergence is in the process of causing a reversal of subduction  
234 polarity, with Eurasian oceanic lithosphere starting to subduct below North Africa<sup>45</sup>: inception of slab pull  
235 may at some stage in the future drive the next dynamic response.

236 Through combining dynamic causes and effects predicted by physics-based modelling with  
237 geologically documented kinematic evolution, we show that plate motion and plate boundary change  
238 induced by one trigger may become the driver of a subsequent plate reorganization event. Such plate  
239 tectonic chain reactions thus allow for long-term propagation of plate tectonic changes through a plate  
240 circuit and provide an avenue towards a dynamic underpinning of intriguing yet hitherto enigmatic global  
241 plate reorganizations. The plate tectonic chain reaction that we identify here propagated from a plate  
242 reorganization induced by mantle plume rise in the southwest Indian ocean to active subduction initiation  
243 in the western Mediterranean region over a time period of ~100 Ma (Fig. 4). We foresee that, on the one  
244 hand, ‘global’ plate reorganizations<sup>5</sup> may in fact be particularly rapid (i.e., within a few million years)  
245 plate tectonic chain reactions initiated by a single trigger<sup>5,7</sup> that sets off a cascade of geodynamic events  
246 propagating through the global plate circuit. On the other hand, they may be a mere coincidence of  
247 several regional chain reactions responding to multiple unrelated triggers. Our analysis illustrates how the  
248 global plate circuit may be tied into self-perpetuating chain of events and paves the way towards a  
249 mechanistic understanding of regional and global plate reorganizations.

250

## 251 **Keywords**

252 Africa-Eurasia convergence, plate kinematics, double subduction, plate reorganization, Neotethys,  
253 Cretaceous Normal Superchron, Cretaceous quiet zone, Central Atlantic, marine magnetic anomalies

254

## 255 **Authors’ information**

256 <sup>1</sup> Department of Earth Sciences, Utrecht University, 3584 CD Utrecht, The Netherlands

257 <sup>2</sup> School of Earth and Environmental Sciences, University of Queensland, St. Lucia, QLD 4072, Australia

258 <sup>3</sup> Department of Earth and Environmental Sciences, Ben-Gurion University of the Negev, Beer-Sheva  
259 84105, Israel

260 \*e-mail: derya.guerer@uq.edu.au

261

262 **Acknowledgements**

263 RG acknowledges ISF grant 716/16. DJJvH acknowledges NWO Vici grant 865.17.001.

264

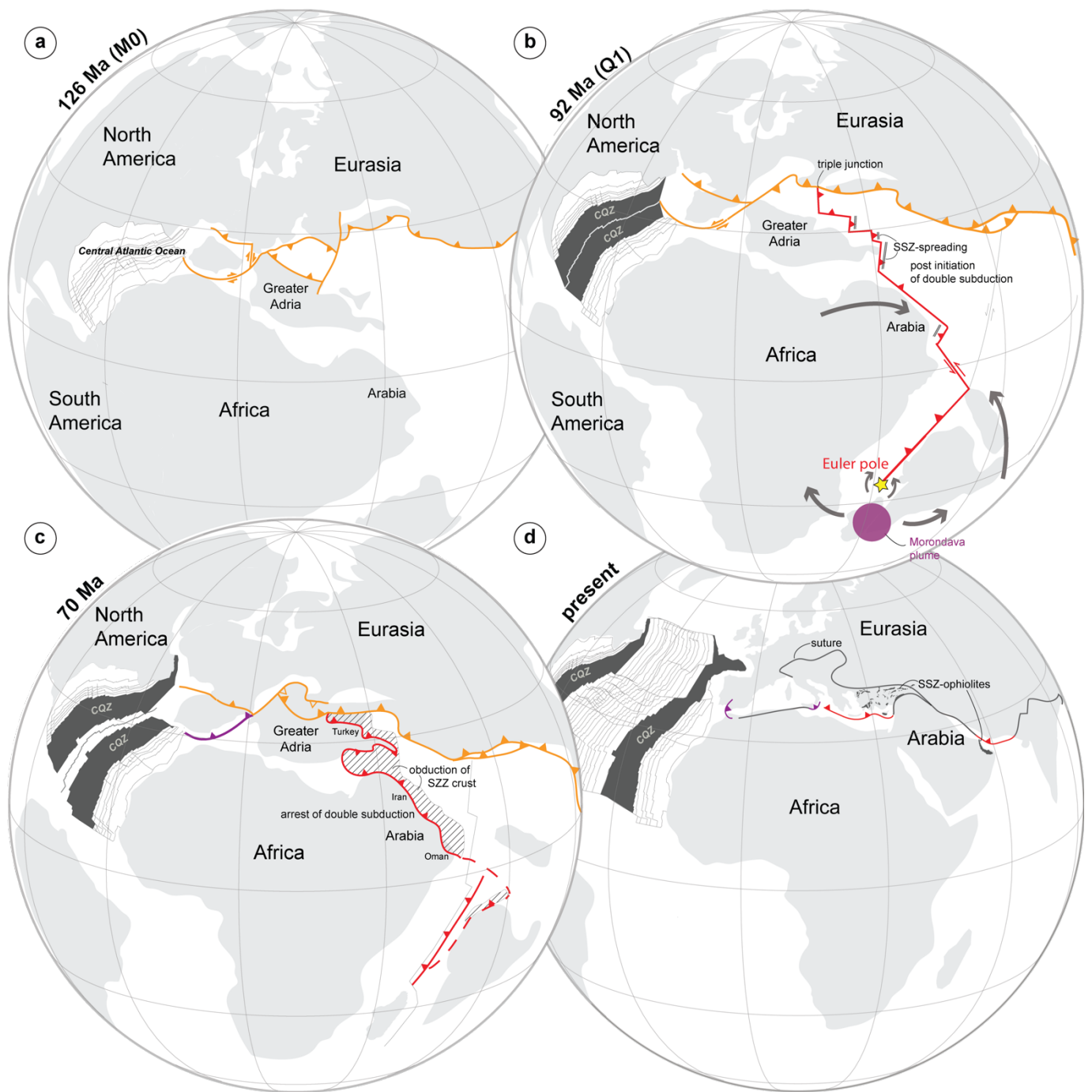
265 **Authors' contributions**

266 All authors contributed equally to the design of the research, the conduction of research, and the writing  
267 of the paper.

268

269 **Competing interests**

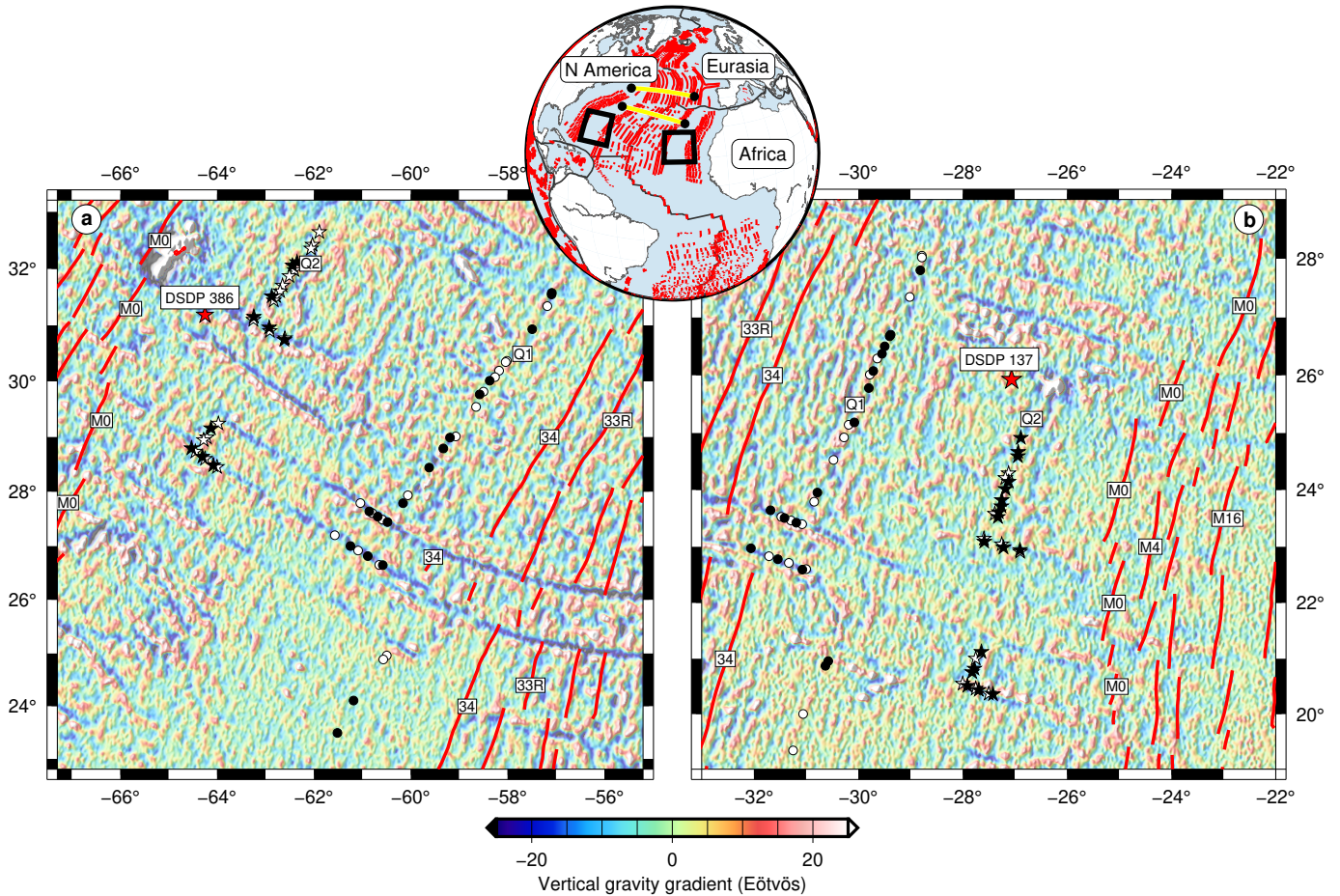
270 The authors declare no competing interests. Correspondence and requests for materials should be  
271 addressed to DG, derya.guerer@uq.edu.au



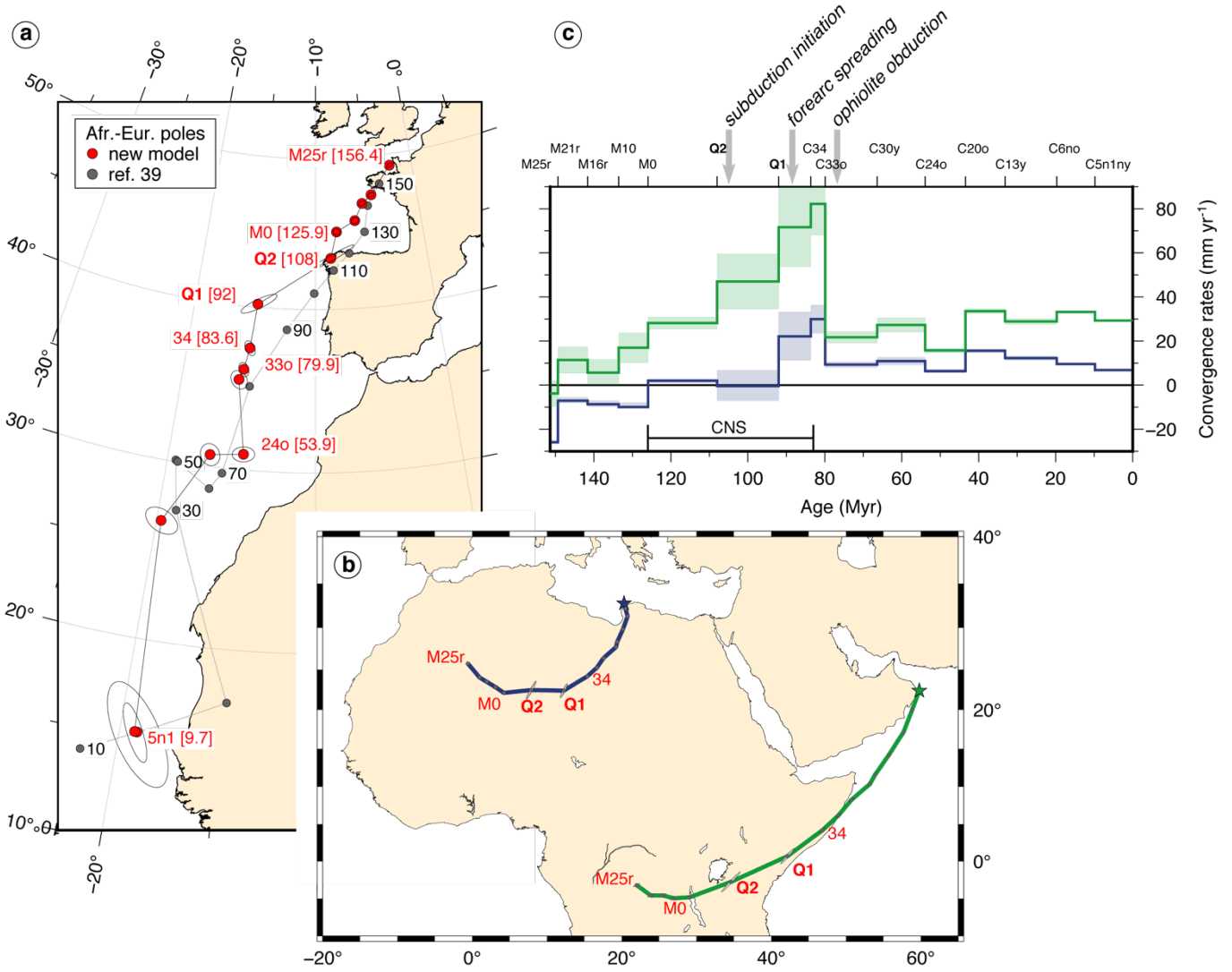
272

273 **Figure 1.** Plate boundary evolution of the Atlantic Ocean, updating previous reconstructions<sup>3</sup> with our  
 274 new constraints in the Neotethys between Africa and Eurasia at a) 126 Ma (corresponding to Anomaly  
 275 M0 - the onset of the Cretaceous Normal Superchron), b) 92 Ma (corresponding to Q1, and around the  
 276 onset of significant slab pull of the Neotethyan intra-oceanic subduction system recorded in eastern  
 277 Mediterranean and Arabian ophiolites), triggered by the arrival of the Morondava plume<sup>11</sup> c) 70 Ma  
 278 (corresponding to obduction of supra-subduction crust (hatched area) and arrest of subduction at the  
 279 Neotethyan intra-oceanic subduction zone along Arabia and NE Africa), and the formation of a new

280 subduction zone in the western Mediterranean (purple) and d) present-day configuration with distribution  
 281 of Neotethyan ophiolites. Reconstructions portrayed in a slab-fitted mantle reference frame<sup>46</sup>. See  
 282 Methods for details. Abbreviations: SSZ, supra-subduction; CQZ, Cretaceous quiet zone.  
 283



284  
 285 **Figure 2.** Central Atlantic Cretaceous quiet zones (**a** North America, **b** Africa) magnetic anomaly and  
 286 fracture zone picks that were used to compute Cretaceous Normal Superchron pole parameters (Q1,  
 287 circles; Q2, stars). White and black symbols delineate the location of the picks and reconstructed picks,  
 288 respectively (wiggle plots are shown in the Extended Data, Fig. 1). Magnetic isochrons are shown with  
 289 red lines. Locations of DSDP drill holes that were used to date Q1 and Q2<sup>21</sup> are marked by red stars.  
 290 Background is the seafloor fabric as delineated by the vertical gravity gradient grids derived from satellite  
 291 altimetry<sup>47</sup>. Note the curvature in fracture zone orientations found toward the young-end of the quiet  
 292 zones. Red lines mark locations of the reversals-related magnetic isochrons. Inset shows the Africa-North  
 293 America-Eurasia plate circuit (yellow lines).

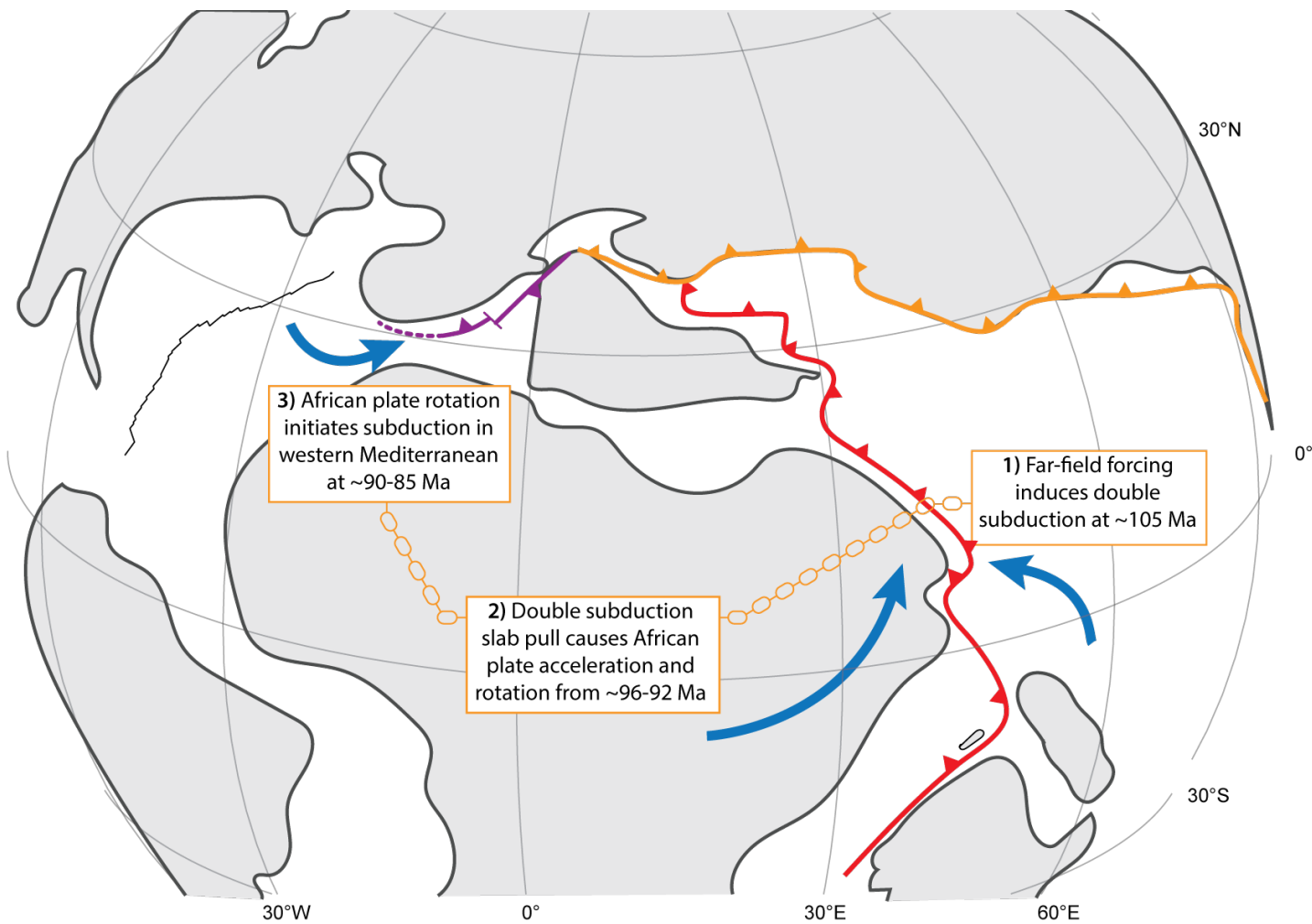


294

295 **Figure 3.** Africa-Eurasia relative plate motions since the Mesozoic. **a.** Location of Africa-Eurasia finite  
 296 rotation poles (red circles) and their 95% confidence ellipses. **b.** Predicted plate motion trajectories for the  
 297 African Plate relative to Eurasian Plate calculated based on our revised kinematic model. The western  
 298 trajectory (blue line) is based on Africa-Eurasia pole parameters whereas the eastern (green line)  
 299 trajectory also includes the Neogene Arabia-Africa motion (see Methods). Grey filled ellipses delineate  
 300 the 95% confidence locations. **c.** Convergence rates computed along the synthetic trajectories. Shadings  
 301 show the 1σ uncertainties. Grey shadings indicate tectonic events.

302

303



304

305 **Figure 4.** Chain of tectonic events in the Neotethys that lead to African-Eurasia plate motion changes as  
 306 the dynamic response to 1) induced subduction initiation at ~104 Ma, followed by 2) the ~96-92 Ma onset  
 307 of African plate acceleration and rotation caused by double in-line slab pull, leading to 3) subduction  
 308 initiation in the western Mediterranean at ~90-85 and finally, ~85-70 Ma arrest of double, in-line slab  
 309 pull.

310

311 **Methods**

312

313 **Timescale**

314 We adopt the time scale of Gradstein et al.<sup>20</sup> because it intercalibrated, among others, bio- and  
 315 magnetostratigraphy. The onset of the CNS (i.e., Anomaly M0) in that timescale is assigned with the age

316 of ~126 Ma, but this age is rather uncertain and the actual age may in fact lay closer to ~121 Myr ago<sup>4,48</sup>.  
317 Because we compare geological events and reconstructions of the Neotethys, largely based on  
318 biostratigraphic dating, with marine magnetic anomalies, our study requires an inter-calibrated timescale  
319 explaining our choice for the Gradstein et al.<sup>20</sup> timescale. We note that shifting the age of the base of the  
320 CNS to ~121 Myr ago would have negligible effect on the convergence rates prior to Q1 (92 Ma ago) as  
321 the direction of Africa-Eurasia relative plate motion nearly paralleled the margin at that time. The ages of  
322 Q1 and Q2 were supported by dated oldest sediments from the ocean floor close to these anomalies  
323 (DSDP sites 137 and 386, Fig. 2), and seafloor spreading model between Anomalies M0 and C34<sup>21</sup>, and  
324 are thus only slightly (i.e., to within a ~million years) affected by the age of the base of the CNS.

325

### 326 **Neotethys reconstruction**

327 The paleo-tectonic map at 92 Ma ago shown in Fig. 1 is based on a systematic kinematic restoration of  
328 plate motions, orogenic deformation, and paleomagnetically-constrained rotations. Restoration of orogens  
329 in the Mediterranean region<sup>22,23,31</sup>, Iran<sup>49</sup> and Oman<sup>26</sup> are based on quantitative structural geological  
330 constraints on reconstruction of back-arc extension, transform motion, shortening, and paleomagnetic  
331 data, in that order. The amount of shortening associated with stacking of orogenic nappes, and the  
332 reconstructed paleogeographic width of the platforms and basins from which these nappes were derived,  
333 is based on the amount of plate convergence constrained from the plate circuit that occurred during the  
334 underthrusting of the nappes as constrained by stratigraphic, metamorphic, and sedimentological data,  
335 whereby the amount of geologically documented shortening is used as a minimum value<sup>22,44</sup>.

336 Reconstructions are tested against and iteratively improved using paleomagnetic constraints on vertical  
337 axis rotations, while obeying structural geological data. Intra-oceanic plate motion and original intra-  
338 oceanic trench motion is constrained from paleomagnetic data on paleolatitude and paleo-dyke  
339 orientations preserved in supra-subduction zone ophiolites of Anatolia, Cyprus, Syria, and Oman<sup>26,31,50</sup>.  
340 Initiation of intra-oceanic subduction from Oman to Turkey is constrained by Lu/Hf garnet crystallization

341 ages of the metamorphic soles of ophiolites of Oman and Anatolia that consistently reveal ~104 Ma  
342 ages<sup>18,30</sup>. Initiation of supra-subduction zone spreading follows from zircon U/Pb ages from gabbros and  
343 plagiogranites in the ophiolites, showing ~96-95 Ma ages for Oman<sup>24</sup> and ~92-90 Ma ages for Anatolia  
344 and Cyprus<sup>25,50</sup>. Predicted locations of subducted slabs at the moment of their breakoff, rotated in a  
345 mantle reference frame<sup>51</sup> are consistent with the locations of subducted slabs in the underlying mantle  
346 constrained from seismic tomography<sup>32,52</sup>. Reconstructions were made in GPlates plate reconstruction  
347 software<sup>53</sup> and all rotation and shape files were provided as supplementary information to previous  
348 papers<sup>22,26,49,54</sup> available at <http://www.geologist.nl/reconstructions/>.

349

### 350 **Africa-North America plate motion**

351 We employed and adopted the results of kinematic investigations that used a best-fitting criteria<sup>55</sup> and  
352 statistical approach<sup>56</sup> to compute the rotation parameters and their uncertainties for a set of plate-pairs.  
353 For the post-CNS period, we adopted the North America-Africa kinematic solutions of Merkuriev and  
354 DeMets<sup>57</sup> and Müller et al.<sup>58</sup> The available Mesozoic kinematic solutions lack uncertainties, therefore we  
355 re-computed the M0, M10, M16r, M21r and M25r finite rotation parameters using the magnetic picks of  
356 Klitgord and Schouten<sup>59,60</sup>, for which we added fracture zone crossings based on satellite gravity data<sup>47</sup>.  
357 We also computed two internal rotation parameters for the Cretaceous Normal Superchron based on  
358 identification of magnetic anomalies (Q1 and Q2, Fig. 1 and Extended Data Fig. 1) that have arisen due to  
359 prominent changes in the behaviour of the geomagnetic field<sup>21</sup>. These features were previously used to  
360 compute the plate kinematics for the Cretaceous South Atlantic Ocean (Africa-South America Plates<sup>61</sup>)  
361 and resulted in opening ages of the Equatorial Atlantic that are consistent with global isotopic signatures  
362 of benthic foraminifera<sup>56</sup>. We here follow a similar approach and internally date the Central Atlantic  
363 CQZs by tracing these two magnetic features based on the available sea surface marine magnetic data (see  
364 Extended Data Fig. 1). Satellite-derived gravity grids now have sufficient accuracy to trace seafloor fabric  
365 (i.e., abyssal hills<sup>47</sup>), which provides additional independent constraint on the orientation of the isochrons.  
366 The new Q1 and Q2 Africa-North America kinematic solutions, with their 95% uncertainty intervals, are

367 shown in Extended Data Fig. 2 and Table 2. Most of the values of the statistical parameter ( $\hat{\kappa}$ ) are near  
368 one (see Extended Data Table 2) indicating that the uncertainty assigned to the data points (magnetic and  
369 fracture zone picks were assigned 4 and 5 km, respectively) used to calculate the solutions were  
370 reasonable<sup>56</sup>. For anomaly Q2 the value of  $\hat{\kappa}$  is 5.5 indicating that the error values for the picks were  
371 overestimated by a factor of 2.3. We note that rescaling the error estimates would make only a minor  
372 difference in the size of the uncertainty ellipse.

373

#### 374 **North America- Eurasia plate motion**

375 We adopted the Eurasia-North America Cenozoic kinematic solutions of Merkouriev and DeMets<sup>41</sup> and  
376 Gaina et al.<sup>62</sup>. The solution for C30y was interpolated using C25y and C31y solutions. The complex  
377 transition from continental rifting to ultra-slow seafloor spreading that occurred during the CNS prevent  
378 us from confidently recognizing the internal quiet zone anomalies. We thus adopted the M25 rotation pole  
379 of Torsvik et al.<sup>63</sup> of which its location is based on seafloor data of the oldest magnetic anomaly and its  
380 angle was extended to bring the paleomagnetic poles of Eurasia and North America to fit. The rotation  
381 parameters of M21r, M16r, M10, M0, Q2, and Q1 were interpolated using C34 and M25 kinematic  
382 solutions<sup>62-64</sup>. Since very slow extensional rates prevailed at this pre-seafloor spreading stage, the  
383 locations of the interpolated Mesozoic poles (and their uncertainties) have negligible effect on the  
384 resultant Africa-Eurasia finite rotation poles.

385

#### 386 **Africa-North America-Eurasia plate circuit**

387 Mesozoic and Cenozoic motions of the African Plate relative to Eurasia Plate were calculated through the  
388 Africa-North America-Eurasia plate circuit. Finite rotations, and their uncertainties, were combined<sup>65</sup> for  
389 the kinematic solutions (Fig. 3 and Extended Data Table 2) giving temporal resolution of ~10 Ma  
390 throughout the studied period (the last 156 Ma). The eastern-most part of Africa is now located on the  
391 Arabian Plate thus in order to calculate the trajectories and relative velocities of the area that is now part  
392 of Arabia, we added published Arabian-African rotation poles<sup>57</sup>.

393 **References**

- 394 1. Torsvik, T. H., Müller, R. D., Van der Voo, R., Steinberger, B. & Gaina, C. Global plate motion  
 395 frames: toward a unified model. *Rev. Geophys.* **46**, (2008).
- 396 2. Matthews, K. J., Seton, M. & Müller, R. D. A global-scale plate reorganization event at 105–100 Ma.  
 397 *Earth Planet. Sci. Lett.* **355–356**, 283–298 (2012).
- 398 3. Müller, R. D. *et al.* Ocean basin evolution and global-scale plate reorganization events since Pangea  
 399 breakup. *Annu. Rev. Earth Planet. Sci.* **44**, 107–138 (2016).
- 400 4. Olierook, H. K. H. *et al.* Timing and causes of the mid-Cretaceous global plate reorganization event.  
 401 *Earth Planet. Sci. Lett.* **534**, 116071 (2020).
- 402 5. Rona, P. A. & Richardson, E. S. Early Cenozoic global plate reorganization. *Earth Planet. Sci. Lett.*  
 403 **40**, 1–11 (1978).
- 404 6. O’Connor, J. M. *et al.* Constraints on past plate and mantle motion from new ages for the Hawaiian-  
 405 Emperor Seamount Chain. *Geochem. Geophys. Geosystems* **14**, 4564–4584 (2013).
- 406 7. Seton, M. *et al.* Ridge subduction sparked reorganization of the Pacific plate-mantle system 60-50  
 407 million years ago: Pacific plate-mantle reorganization. *Geophys. Res. Lett.* **42**, 1732–1740 (2015).
- 408 8. Whittaker, J. M. *et al.* Major Australian-Antarctic plate reorganization at Hawaiian-Emperor bend  
 409 time. *Science* **318**, 83–86 (2007).
- 410 9. Cande, S. C. & Stegman, D. R. Indian and African plate motions driven by the push force of the  
 411 Reunion plume head. *Nature* **475**, 47–52 (2011).
- 412 10. van Hinsbergen, D. J., Steinberger, B., Doubrovine, P. V. & Gassmöller, R. Acceleration and  
 413 deceleration of India-Asia convergence since the Cretaceous: Roles of mantle plumes and continental  
 414 collision. *J. Geophys. Res. Solid Earth* **116**, (2011).
- 415 11. van Hinsbergen, D. J. *et al.* A record of plume-induced plate rotation triggering seafloor spreading  
 416 and subduction initiation. (2021).
- 417 12. Jagoutz, O., Royden, L., Holt, A. F. & Becker, T. W. Anomalously fast convergence of India and  
 418 Eurasia caused by double subduction. *Nat. Geosci.* **8**, 475–478 (2015).

- 419 13. Faccenna, C., Becker, T. W., Lallemand, S. & Steinberger, B. On the role of slab pull in the Cenozoic  
420 motion of the Pacific plate. *Geophys. Res. Lett.* **39**, L03305 (2012).
- 421 14. Domeier, M. *et al.* Intraoceanic subduction spanned the Pacific in the Late Cretaceous–Paleocene.  
422 *Sci. Adv.* **3**, eaao2303 (2017).
- 423 15. Buitter, S. J. & Torsvik, T. H. A review of Wilson Cycle plate margins: A role for mantle plumes in  
424 continental break-up along sutures? *Gondwana Res.* **26**, 627–653 (2014).
- 425 16. Stern, R. J. Subduction initiation: spontaneous and induced. *Earth Planet. Sci. Lett.* **226**, 275–292  
426 (2004).
- 427 17. Wu, J. T.-J. & Wu, J. Izanagi-Pacific ridge subduction revealed by a 56 to 46 Ma magmatic gap along  
428 the northeast Asian margin. *Geology* **47**, 953–957 (2019).
- 429 18. Guilmette, C. *et al.* Forced subduction initiation recorded in the sole and crust of the Semail Ophiolite  
430 of Oman. *Nat. Geosci.* **11**, 688–695 (2018).
- 431 19. Agard, P., Jolivet, L., Vrielynck, B., Burov, E. & Monie, P. Plate acceleration: the obduction trigger?  
432 *Earth Planet. Sci. Lett.* **258**, 428–441 (2007).
- 433 20. Gradstein, F. M., Ogg, J. G., Schmitz, M. & Ogg, G. *The geologic time scale 2012*. (Elsevier, 2012).
- 434 21. Granot, R., Dyment, J. & Gallet, Y. Geomagnetic field variability during the Cretaceous Normal  
435 Superchron. *Nat. Geosci.* **5**, 220–223 (2012).
- 436 22. van Hinsbergen, D. J. J. *et al.* Orogenic architecture of the Mediterranean region and kinematic  
437 reconstruction of its tectonic evolution since the Triassic. *Gondwana Res.* **81**, 79–229 (2020).
- 438 23. Gürer, D., van Hinsbergen, D. J. J., Matenco, L., Corfu, F. & Cascella, A. Kinematics of a former  
439 oceanic plate of the Neotethys revealed by deformation in the Ulukışla basin (Turkey). *Tectonics* **35**,  
440 2385–2416 (2016).
- 441 24. Rioux, M. *et al.* Tectonic development of the Semail ophiolite: High-precision U-Pb zircon  
442 geochronology and Sm-Nd isotopic constraints on crustal growth and emplacement. *J. Geophys. Res.*  
443 **118**, 2085–2101 (2013).
- 444 25. Parlak, O. The Tauride ophiolites of Anatolia (Turkey): A review. *J. Earth Sci.* **27**, 901–934 (2016).

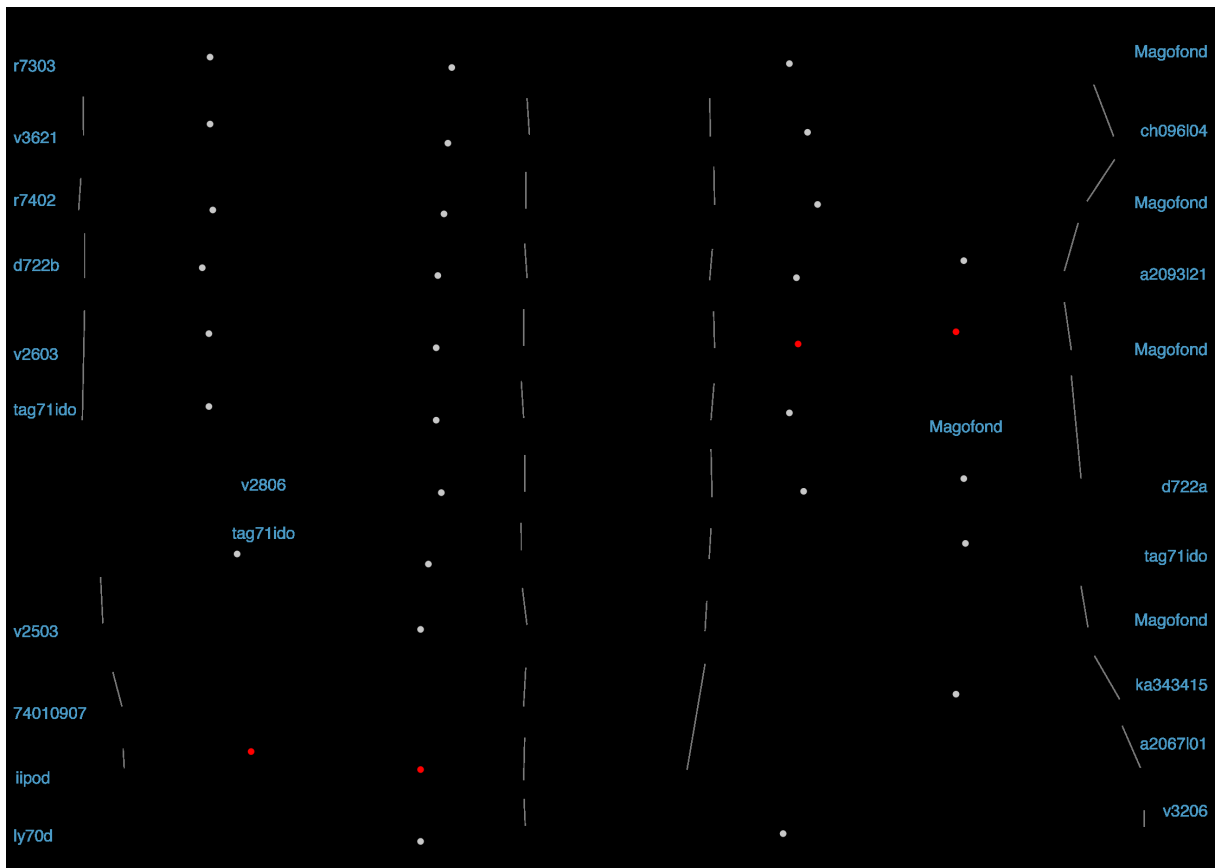
- 445 26. van Hinsbergen, D. J. J., Maffione, M., Koornneef, L. M. & Guilmette, C. Kinematic and  
446 paleomagnetic restoration of the Semail ophiolite (Oman) reveals subduction initiation along an  
447 ancient Neotethyan fracture zone. *Earth Planet. Sci. Lett.* **518**, 183–196 (2019).
- 448 27. Gaina, C. & Jakob, J. Global eocene tectonic unrest: Possible causes and effects around the North  
449 American plate. *Tectonophysics* **760**, 136–151 (2019).
- 450 28. Schellart, W. P. Andean mountain building and magmatic arc migration driven by subduction-induced  
451 whole mantle flow. *Nat. Commun.* **8**, 1–13 (2017).
- 452 29. Tavani, S., Corradetti, A., Sabbatino, M., Seers, T. & Mazzoli, S. Geological record of the transition  
453 from induced to self-sustained subduction in the Oman Mountains. *J. Geodyn.* **133**, 101674 (2020).
- 454 30. Pourteau, A. *et al.* Thermal evolution of an ancient subduction interface revealed by Lu–Hf garnet  
455 geochronology, Halilbağı Complex (Anatolia). *Geosci. Front.* **10**, 127–148 (2019).
- 456 31. Maffione, M., van Hinsbergen, D. J. J., de Gelder, G. I. N. O., van der Goes, F. C. & Morris, A.  
457 Kinematics of Late Cretaceous subduction initiation in the Neo-Tethys Ocean reconstructed from  
458 ophiolites of Turkey, Cyprus, and Syria. *J. Geophys. Res.* **122**, 3953–3976 (2017).
- 459 32. van der Meer, D. G., van Hinsbergen, D. J. J. & Spakman, W. Atlas of the underworld: Slab remnants  
460 in the mantle, their sinking history, and a new outlook on lower mantle viscosity. *Tectonophysics* **723**,  
461 309–448 (2018).
- 462 33. Warren, C. J., Parrish, R. R., Waters, D. J. & Searle, M. P. Dating the geologic history of Oman’s  
463 Semail ophiolite: insights from U-Pb geochronology. *Contrib. Mineral. Petrol.* **150**, 403–422 (2005).
- 464 34. Holt, A. F., Royden, L. H. & Becker, T. W. The dynamics of double slab subduction. *Geophys. J. Int.*  
465 **209**, 250–265 (2017).
- 466 35. Čížková, H. & Bina, C. R. Geodynamics of trench advance: Insights from a Philippine-Sea-style  
467 geometry. *Earth Planet. Sci. Lett.* **430**, 408–415 (2015).
- 468 36. Pusok, A. E. & Stegman, D. R. Formation and Stability of Same-Dip Double Subduction Systems. *J.*  
469 *Geophys. Res.* **124**, 7387–7412 (2019).

- 470 37. Király, Á., Funicello, F., Capitanio, F. A. & Faccenna, C. Dynamic interactions between subduction  
471 zones. *Glob. Planet. Change* 103501 (2021).
- 472 38. Dewey, J. F., Helman, M. L., Knott, S. D., Turco, E. & Hutton, D. H. W. Kinematics of the western  
473 Mediterranean. *Geol. Soc. Lond. Spec. Publ.* **45**, 265–283 (1989).
- 474 39. Rosenbaum, G., Lister, G. S. & Duboz, C. Relative motions of Africa, Iberia and Europe during  
475 Alpine orogeny. *Tectonophysics* **359**, 117–129 (2002).
- 476 40. Péron-Pinvidic, G., Manatschal, G., Minshull, T. A. & Sawyer, D. S. Tectonosedimentary evolution  
477 of the deep Iberia-Newfoundland margins: Evidence for a complex breakup history. *Tectonics* **26**,  
478 (2007).
- 479 41. Merkouriev, S. & DeMets, C. A high-resolution model for Eurasia–North America plate kinematics  
480 since 20 Ma. *Geophys. J. Int.* **173**, 1064–1083 (2008).
- 481 42. Lahondère, D. & Guerrot, C. Datation Sm-Nd du métamorphisme éclogitique en Corse alpine: un  
482 argument pour l'existence au Crétacé supérieur d'une zone de subduction active localisée sous le bloc  
483 corso-sarde. *Géologie Fr.* 3–11 (1997).
- 484 43. Manzotti, P., Ballèvre, M., Zucali, M., Robyr, M. & Engi, M. The tectonometamorphic evolution of  
485 the Sesia–Dent Blanche nappes (internal Western Alps): review and synthesis. *Swiss J. Geosci.* **107**,  
486 309–336 (2014).
- 487 44. Chertova, M. V., Spakman, W., Geenen, T., van den Berg, A. P. & van Hinsbergen, D. J. J.  
488 Underpinning tectonic reconstructions of the western Mediterranean region with dynamic slab  
489 evolution from 3-D numerical modeling. *J. Geophys. Res.* **119**, 5876–5902 (2014).
- 490 45. Hamai, L. *et al.* Towards subduction inception along the inverted North African margin of Algeria?  
491 Insights from thermo-mechanical models. *Earth Planet. Sci. Lett.* **501**, 13–23 (2018).
- 492 46. van der Meer, D. G., Spakman, W., van Hinsbergen, D. J. J., Amaru, M. L. & Torsvik, T. H. Towards  
493 absolute plate motions constrained by lower-mantle slab remnants. *Nat. Geosci.* **3**, 36–40 (2010).
- 494 47. Sandwell, D. T., Müller, R. D., Smith, W. H. F., Garcia, E. & Francis, R. New global marine gravity  
495 model from CryoSat-2 and Jason-1 reveals buried tectonic structure. *Science* **346**, 65–67 (2014).

- 496 48. Midtkandal, I. *et al.* The Aptian (Early Cretaceous) oceanic anoxic event (OAE1a) in Svalbard,  
497 Barents Sea, and the absolute age of the Barremian-Aptian boundary. *Palaeogeogr. Palaeoclimatol.*  
498 *Palaeoecol.* **463**, 126–135 (2016).
- 499 49. McQuarrie, N. & van Hinsbergen, D. J. J. Retrodeforming the Arabia-Eurasia collision zone: Age of  
500 collision versus magnitude of continental subduction. *Geology* **41**, 315–318 (2013).
- 501 50. van Hinsbergen, D. J. J. *et al.* Tectonic evolution and paleogeography of the Kırşehir Block and the  
502 Central Anatolian Ophiolites, Turkey. *Tectonics* **35**, 983–1014 (2016).
- 503 51. Doubrovine, P. V., Steinberger, B. & Torsvik, T. H. Absolute plate motions in a reference frame  
504 defined by moving hot spots in the Pacific, Atlantic, and Indian oceans. *J. Geophys. Res.* **117**, (2012).
- 505 52. Gürer, M. D. Subduction evolution in the Anatolian region: the rise, demise, and fate of the Anadolu  
506 Plate. (Utrecht University, The Netherlands, 2017).
- 507 53. Boyden, J. A. *et al.* Next-generation plate-tectonic reconstructions using GPlates. in *Geoinformatics:*  
508 *Cyberinfrastructure for the Solid Earth Sciences* (eds. Keller, G. R. & Baru, C.) 95–113 (Cambridge  
509 University Press, 2011).
- 510 54. Gürer, D. & van Hinsbergen, D. J. J. Diachronous demise of the Neotethys Ocean as a driver for non-  
511 cylindrical orogenesis in Anatolia. *Tectonophysics* **760**, 95–106 (2019).
- 512 55. Hellinger, S. J. The uncertainties of finite rotations in plate tectonics. *J. Geophys. Res.* **86**, 9312–9318  
513 (1981).
- 514 56. Royer, J.-Y. & Chang, T. Evidence for relative motions between the Indian and Australian Plates  
515 during the last 20 m.y. from plate tectonic reconstructions: Implications for the deformation of the  
516 Indo-Australian Plate. *J. Geophys. Res.* **96**, 11779–11802 (1991).
- 517 57. Merkouriev, S. & DeMets, C. High-resolution estimates of Nubia–North America plate motion: 20  
518 Ma to present. *Geophys. J. Int.* **196**, 1281–1298 (2013).
- 519 58. Müller, R. D., Royer, J.-Y., Cande, S. C., Roest, W. R. & Maschenkov, S. New constraints on the  
520 Late Cretaceous/Tertiary plate tectonic evolution of the Caribbean. in *Sedimentary Basins of the*  
521 *World* (ed. Mann, P.) vol. 4 33–59 (Elsevier, 1999).

- 522 59. Klitgord, K. D. & Schouten, H. Plate kinematics of the central Atlantic. in *The Western North Atlantic*  
523 *Region* (eds. Vogt, P. R. & Tucholke, B. E.) 351–378 (Geology of North America, 1986).  
524 doi:10.1130/DNAG-GNA-M.351.
- 525 60. Seton, M. *et al.* Community infrastructure and repository for marine magnetic identifications.  
526 *Geochem. Geophys. Geosystems* **15**, 1629–1641 (2014).
- 527 61. Granot, R. & Dymant, J. The Cretaceous opening of the South Atlantic Ocean. *Earth Planet. Sci. Lett.*  
528 **414**, 156–163 (2015).
- 529 62. Gaina, C., Roest, W. R. & Müller, R. D. Late Cretaceous–Cenozoic deformation of northeast Asia.  
530 *Earth Planet. Sci. Lett.* **197**, 273–286 (2002).
- 531 63. Torsvik, T. H., Van der Voo, R., Meert, J. G., Mosar, J. & Walderhaug, H. J. Reconstructions of the  
532 continents around the North Atlantic at about the 60th parallel. *Earth Planet. Sci. Lett.* **187**, 55–69  
533 (2001).
- 534 64. Doubrovine, P. V. & Tarduno, J. A. A revised kinematic model for the relative motion between  
535 Pacific oceanic plates and North America since the Late Cretaceous. *J. Geophys. Res.* **113**, B12101  
536 (2008).
- 537 65. Chang, T., Stock, J. & Molnar, P. The rotation group in plate tectonics and the representation of  
538 uncertainties of plate reconstructions. *Geophys. J. Int.* **101**, 649–661 (1990).  
539





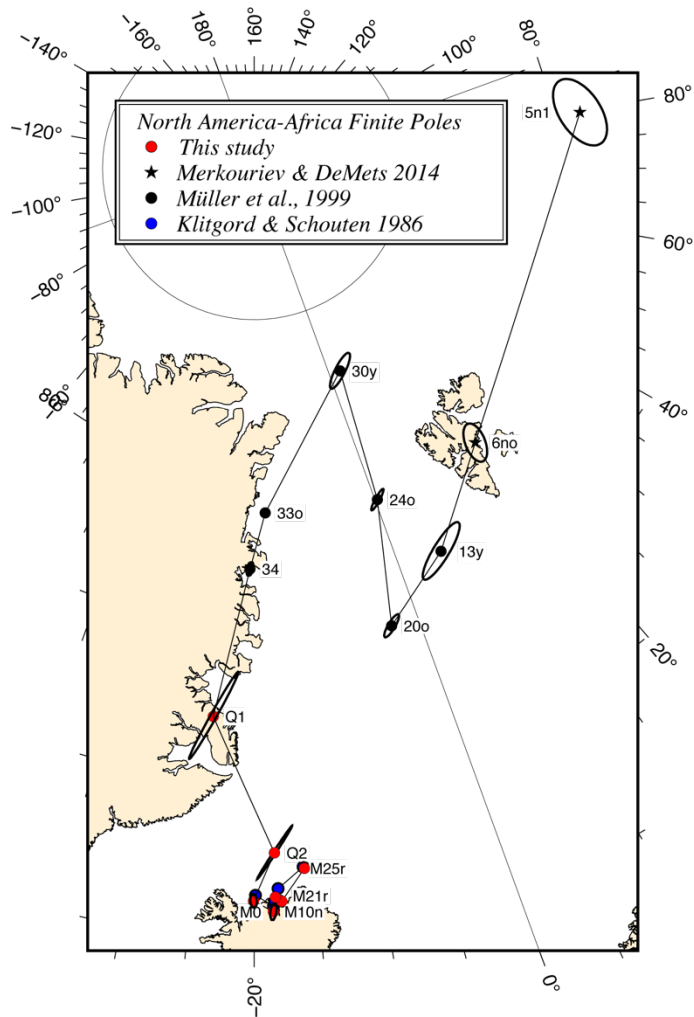
12

13 **Figure 1.** Magnetic anomaly sea surface representative profiles used for the kinematic analysis  
 14 of the Central Atlantic quiet zones ordered from north (top) to south (bottom). Magnetic  
 15 identification of Q1 and Q2 are shown in two profiles with red circles<sup>6</sup>. These anomalies were  
 16 then traced outward into the other Central Atlantic magnetic profiles<sup>6</sup> (gray circles), using both  
 17 the magnetic anomalies backed by the vertical gradient of the gravity field (Fig. 1) that provide  
 18 independent constraints on the crustal structure and seafloor fabric. Sources of data are the  
 19 National Centers for Environmental Information (NCEI) and Ifremer (MAGOFOND cruise<sup>9</sup>).

20

21

22



23

24 **Figure 2.** North America-Africa finite rotation poles and their 95% confidence ellipses.

25

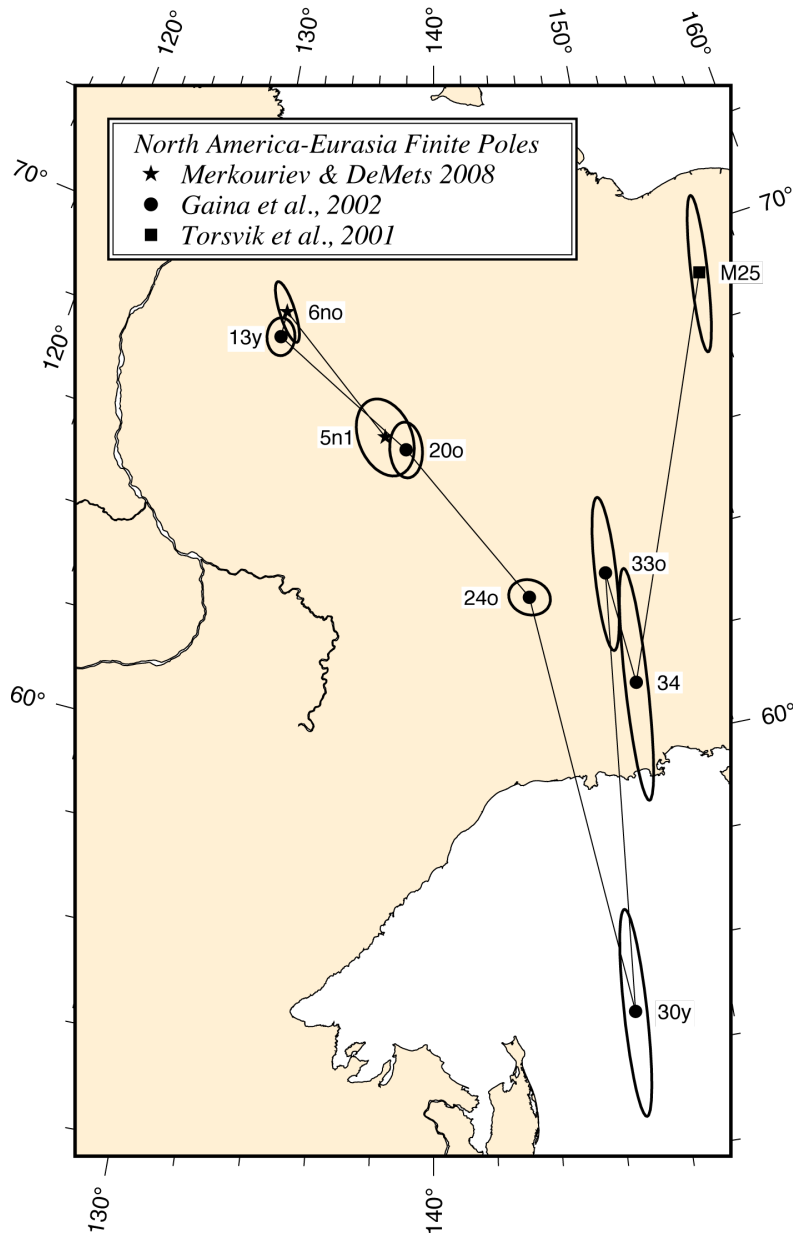
26 **Table 2.** Finite rotations and covariance matrices for the relative motion of Africa relative to  
 27 North America (fixed). The covariance matrix is given by the formula  $\frac{1}{\hat{k}} *$

28  $(a \ b \ c \ b \ d \ e \ c \ e \ f) * 10^{-g}$  radians<sup>2</sup>.

29

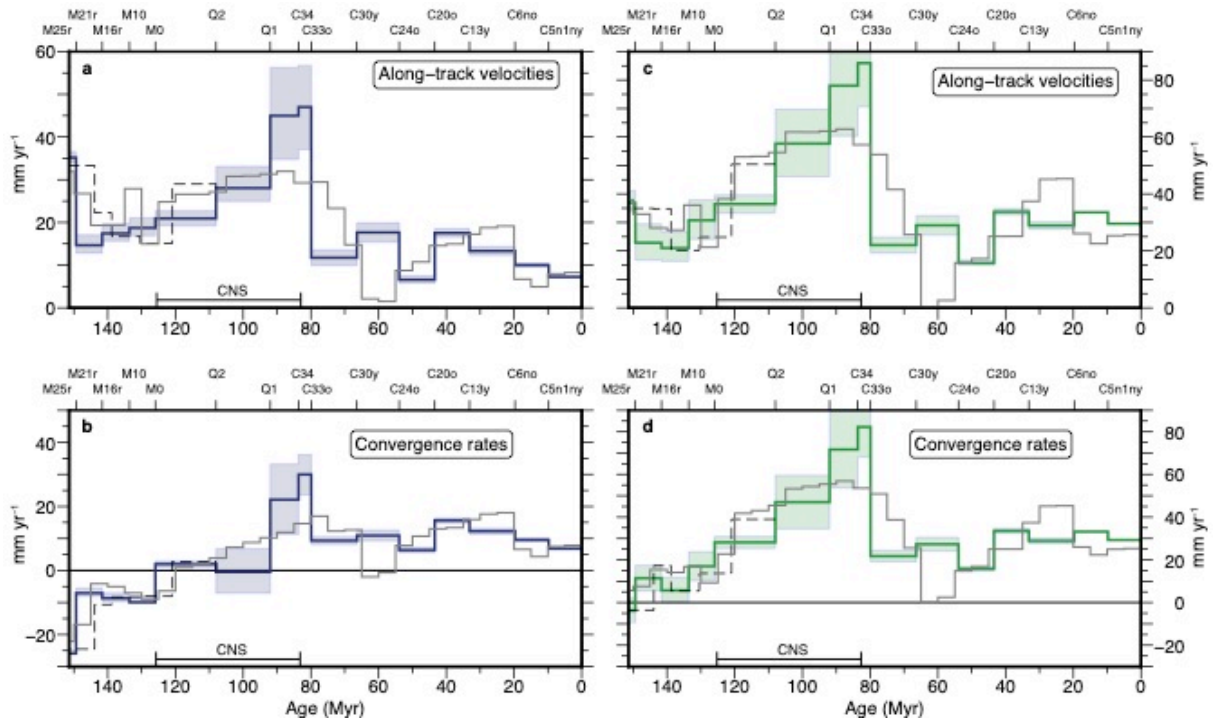
Mag. Ano	Lat (°N)	Long (°E)	Angle (°)	$\hat{k}$	a	b	c	d	e	f	g
Q1	71.98	-24.26	35.88	1.81	2.48	-4.05	2.71	6.69	-4.49	3.02	5
Q2	67.64	-18.30	46.76	5.56	3.70	-7.12	4.82	13.77	-9.33	6.34	5
M0	66.12	-20.05	54.41	0.78	10.52	-7.47	1.91	8.69	-4.65	3.87	7
M10	66.77	-18.52	57.58	0.50	9.90	-9.64	5.14	11.94	-7.27	5.15	7
M16r	66.23	-18.33	59.70	1.02	9.86	-11.08	5.37	15.25	-8.44	5.24	7
M21r	66.10	-17.85	62.12	2.15	13.90	-9.53	1.74	9.89	-4.12	3.07	7
M25r	67.10	-15.90	64.70	1.78	7.60	-6.31	1.39	8.77	-4.21	3.20	7

30



31

32 **Figure 3.** North America- Eurasia finite rotation poles and their 95% confidence ellipses.



33

34 **Figure 4.**

35 Velocities along-track (**a,c**) and convergence rates (**b,d**) for the trajectories shown in Fig. 3b  
 36 (a-b and c-d are calculated using the western and eastern trajectory, respectively). The velocities  
 37 were calculated using the geomagnetic polarity time scale of Ogg<sup>3</sup>. Dashed lines delineate the  
 38 Mesozoic rates when using the Malinverno et al.<sup>7</sup> timescale. Grey lines show previous estimates  
 39 of convergence rates inferred from interpolating plate motion change across the entire  
 40 Cretaceous Normal Superchron<sup>10</sup>. Blue shadings show the  $1\sigma$  uncertainties that were calculated  
 41 based on the uncertainties of the reconstructed points. Convergence rates are the margin-  
 42 orthogonal components of the relative motions, calculated along northward (**b**) or N30°E (**d**)  
 43 direction.

44

45 **References**

- 46 1. Merkouriev, S. & DeMets, C. High-resolution Neogene reconstructions of Eurasia-North  
47 America Plate motion. *Geophys. J. Int.* **198**, 366–384 (2014).
- 48 2. Merkouriev, S. & DeMets, C. A high-resolution model for Eurasia–North America plate  
49 kinematics since 20 Ma. *Geophys. J. Int.* **173**, 1064–1083 (2008).
- 50 3. Ogg, J. G. Geomagnetic polarity time scale. in *The Geologic Time Scale 2012 edited by*  
51 *Gradstein, F. M., Ogg, J. G., Schmitz, M. D. and Ogg, G. M.* 85–114 (Elsevier, 2012).
- 52 4. Müller, R. D., Royer, J.-Y., Cande, S. C., Roest, W. R. & Maschenkov, S. New constraints  
53 on the Late Cretaceous/Tertiary plate tectonic evolution of the Caribbean. in *Sedimentary*  
54 *Basins of the World* (ed. Mann, P.) vol. 4 33–59 (Elsevier, 1999).
- 55 5. Gaina, C., Roest, W. R. & Müller, R. D. Late Cretaceous–Cenozoic deformation of  
56 northeast Asia. *Earth Planet. Sci. Lett.* **197**, 273–286 (2002).
- 57 6. Granot, R., Dyment, J. & Gallet, Y. Geomagnetic field variability during the Cretaceous  
58 Normal Superchron. *Nat. Geosci.* **5**, 220–223 (2012).
- 59 7. Malinverno, A., Hildebrandt, J., Tominaga, M. & Channell, J. E. T. M-sequence  
60 geomagnetic polarity time scale (MHTC12) that steadies global spreading rates and  
61 incorporates astrochronology constraints. *J. Geophys. Res.* **117**, (2012).
- 62 8. Torsvik, T. H., Van der Voo, R., Meert, J. G., Mosar, J. & Walderhaug, H. J.  
63 Reconstructions of the continents around the North Atlantic at about the 60th parallel.  
64 *Earth Planet. Sci. Lett.* **187**, 55–69 (2001).
- 65 9. Dyment J., Gallet Y. MAGOFOND cruise, RV Le Suroît, (2005),  
66 <https://doi.org/10.17600/5020060>, see cruise webpage:  
67 <https://campagnes.flotteoceanographique.fr/campagnes/5020060/>
- 68 10. Rosenbaum, G., Lister, G. S. & Duboz, C. Relative motions of Africa, Iberia and Europe  
69 during Alpine orogeny. *Tectonophysics* **359**, 117–129 (2002).